Patterns and drivers of population trends on individual Breeding Bird Survey routes using spatially explicit models and route-level covariates.

Adam C. Smith, Veronica Aponte, Allison D. Binley, Amelia R. Cox, Lindsay Daly, Courtney Donkersteeg, Brandon P.M. Edwards, Willow B. English, Marie-Anne R. Hudson, David Iles, Kendall Jefferys, Barry Robinson, Christian Roy

Adam C. Smith – adam.smith@ec.gc.ca, Canadian Wildlife Service, Environment and Climate Change Canada, Ottawa, ORCID: 0000-0002-2829-4843

Veronica Aponte - Canadian Wildlife Service, Environment and Climate Change Canada, Ottawa,

Marie-Anne R. Hudson - Canadian Wildlife Service, Environment and Climate Change Canada, Ottawa, ORCID: 0000-0002-9599-0697

Willow B English - Canadian Wildlife Service, Environment and Climate Change Canada, Ottawa, ORCID: 0000-0002-0863-8581

Kendall M Jefferys - Environmental Change Institute, School of Geography and the Environment, University of Oxford, Oxford, UK ORCID: 0000-0003-4439-9394

Allison D. Binley - Department of Biology, Carleton University, Ottawa, Canada ORCID: 0000-0001-8790-9935

Barry Robinson - Canadian Wildlife Service, Environment and Climate Change Canada, Edmonton Canada ORCID: 0000-0002-2646-2508

Courtney Donkersteeg - Department of Biology, Carleton University, Ottawa, Canada

Brandon P.M. Edwards, Department of Biology, Carleton University, Ottawa, Canada & Canadian Wildlife Service, Environment and Climate Change Canada, Ottawa, ORCID: 0000-0003-0865-3076

Lindsay Daly - Canadian Wildlife Service, Environment and Climate Change Canada, Ottawa, ORCID: 0000-0002-0892-5505

Amelia R. Cox - Canadian Wildlife Service, Environment and Climate Change Canada, Yellowknife, Canada

Christian Roy - Canadian Wildlife Service, Environment and Climate Change Canada, Gatineau, Canada ORCID: 0000-0002-5599-6234

Acknowledgements:

We sincerely thank the thousands of U.S. and Canadian participants and the regional and national coordinators who have conducted and coordinated the North American Breeding Bird Survey for almost 60 years.

Data Availability

Analyses reported in this article can be reproduced using the data and code provided at https://github.com/AdamCSmithCWS/Route-level_BBS_trends.

Keywords

Ecological Monitoring, Gaussian Process, iCAR, population abundance

Abstract

Spatial patterns in population trends, particularly those at finer geographic scales, can help us better understand the factors driving population change in North American birds. The standard status and trend models for the North American Breeding Bird Survey (BBS) were designed to estimate trends within broad geographic strata, such as Bird Conservation Regions, U.S. states, and Canadian territories or provinces. Calculating trend estimates at the level of individual survey transects ("routes") from the BBS allows us to explore finer spatial patterns and simultaneously estimate the effects of covariates, such as habitat-loss or annual weather, on both relative abundance and trend (changes in relative abundance through time). Here, we describe four related hierarchical Bayesian models that estimate trends for individual BBS routes, implemented in the probabilistic programing language Stan. All four models estimate route-level trends and relative abundances using a hierarchical structure that shares information among routes, and three of the models share information in a spatially explicit way. The spatial models use either an intrinsic Conditional Autoregressive structure or a distance-based Gaussian process to estimate the spatial components. We fit all four models to data for 71 species and then fit only two of the models (one spatial and one non-spatial) for an additional 216 species due to computational limitations. Leave-future-out cross-validation showed the spatial models outperformed the non-spatial model for 284 out of 287 species. For the species tested here, the best approach to modeling the spatial components depended on the species; the Gaussian Process had the highest predictive accuracy for 2/3 of the species tested here and the iCAR was better for the remaining 1/3. We also present two examples of route-level covariate analyses focused on spatial and temporal variation in habitat for Rufous Hummingbird (*Selasphorus rufus*) and Horned Grebe (*Podiceps auritus*). Covariates explain or affect patterns in the rate of population change for both species. Route-level models for BBS data are useful for visualizing spatial patterns of population change, generating hypotheses on the causes of change, comparing patterns of change among regions and species, and testing hypotheses on causes of change with relevant covariates.

Introduction

The North American Breeding Bird Survey (BBS), is often used to produce regional estimates of population change which inform national and international conservation initiatives. The BBS is a standardized monitoring program that has been running for over 50 years across North America and provides data for up to 500 species (Sauer et al. 2017, Hudson et al. 2017). BBS data are collected by conducting 50, 3-minute point-counts along a 40 km route, with over 5400 routes across North America (Hudson et al. 2017). BBS data are often used to estimate the change in a species' population over time (i.e. trend) across regions such as Bird Conservation Regions (BCRs; Sauer et al. 2003) or the intersection of states/provinces with BCRs (Soykan et al. 2016, Link et al. 2020, Smith and Edwards 2020). These regional-scale summaries have been very useful to identify and prioritize species in peril (Government of Canada 2010, IUCN 2012, Rosenberg et al. 2017) and to understand broad-scale patterns of change in North American birds (North American Bird Conservation Initiative Canada 2019, Rosenberg et al. 2019, North American Bird Conservation Initiative 2022).

Finer-scale models using BBS data are another use of the long-term dataset, which can address different ecological questions and conservation efforts. Many factors influence the relative abundance and trends in bird populations, and they act and interact across a range of spatial scales (Morrison et al. 2010). Spatial patterns in populations can be induced by factors such as habitat change (Stanton et al. 2018, Betts et al. 2022), biotic factors such as prey availability (Drever et al. 2018), or broad-scale patterns in abiotic factors including precipitation, temperature, and phenology (Renfrew et al. 2013, Wilson et al. 2018), and these factors can act or interact within or across different periods in the species' annual cycles (Morrison et al. 2010, Wilson et al. 2011). Likewise, conservation actions occur at many scales, from international conventions, to very fine scales, such as an individual wetland (Prairie Habitat Joint Venture 2020). Fine-scale estimates of population trends may provide a more useful unit for local conservation efforts and a better scale to model covariates with fine-scale effects such as species interactions, local landcover, and agricultural practices (Thogmartin et al. 2004, Paton et al. 2019, Mirochnitchenko et al. 2021). Therefore,

fine-scale estimates of population trends complement the broader-scale estimates and can represent patterns in the factors shaping populations as well as the scales at which conservation is implemented.

The factors affecting population trends may differ from those affecting relative abundance and so it makes sense to model those processes separately. Earlier fine-scale models for the BBS did not explicitly model the rate of population change as a parameter in the model (Bled et al. 2013), although see (Betts et al. 2022). However, a spatially-explicit hierarchical regression can model both spatial patterns in mean relative abundance and the rate of change in relative abundance (Ver Hoef et al. 2018, Wright et al. 2021). Separating these parameters in the model also allows for the inclusion of covariates to better understand the processes affecting local abundance and trends (Meehan et al. 2019).

Spatially explicit models in ecology are well defined to treat individual sample units as either points within continuous space (Golding and Purse 2016), or discrete areas with neighborhood relationships (Ver Hoef et al. 2018). Intrinsic Conditional Autoregressive (iCAR) structures are areal and consider the adjacency between a discrete spatial area and its neighbors (Besag and Kooperberg 1995). These structures have been used to model the relatively fine-scale population trends in Christmas Bird Count data (Meehan et al. 2019) and the annual relative abundance of birds using BBS data (Bled et al. 2013). Gaussian Process (GP) models consider the Euclidean distance between points and can model fine-scale spatial patterns in animal relative abundance, treating spatial distances between survey sites as the basis for modeling the covariance of parameters in space (Golding and Purse 2016).

Here we describe four regression models to 1) estimate bird population trends and relative abundance for each BBS route and 2) visualize spatial patterns in both trend and relative abundance across a species' monitored range. Three of the models share information on relative abundance and trend in a spatially explicit way, while the fourth model lacks any spatial information. We describe two models that rely on an iCAR structure to model the spatial relationships: the first is the iCAR model; which uses only the iCAR structure to model variation in abundance and trends; and the second is the BYM model (Besag York Mollié, (Besag et al. 1991), which is identical to the iCAR model but includes an additional random

effect on the route-level trends to allow extra non-spatial variation in trends. We also describe a GP model that uses an isotropic Gaussian Process to model covariance among routes in the abundance and trends, and finally a non-spatial version of the model that estimates route-level variation in trends and abundances as a simple normally distributed random effect. We fit all models to 71 species, and fit the non-spatial model and the iCAR model to another 216 species, selected based on sufficient data and computational limits (details below). We compare the predictive accuracy of all models for a given species in a leave-future-out cross-validation to assess the benefits of including spatial information. Finally, we provide examples of route-level covariate analyses to demonstrate modifications of these models and the utility of modeling BBS data at a relatively fine, route-level scale.

Methods

Data

We used data for the Baird's Sparrow (Centronyx *bairdii*) as an example species to demonstrate the spatial structures, model fit, and convergence. We chose the Baird's Sparrow as it had sufficient data to produce robust estimates but has a very restricted distribution, confined to the northern Great Plains region (Figure 1), which reduces model run-time. We used data for another 70 species (Table S1) to fit all four of the models and compared the predictions and predictive accuracy among the models. We chose these 70 species (71 including Baird's Sparrow) because they have small ranges with relatively few BBS routes, which minimizes the size of distance matrices and/or adjacency matrices for computational efficiency, and yet also relatively high-quality data on any given route. Specifically, from 2006 to 2021 these small-range species had been observed on 125 - 400 BBS routes, with at least 600 observations of the species (positive counts), and the average number of positive counts per route was greater than four. We could only compare the fit and predictive accuracy of all four models using these species with relatively few data because the time required to fit one of the models (GP) was prohibitive for large inter-route distance matrices. For the additional 216 species that were observed on at least 400 BBS routes during the years 2006 - 2021, we compare the predictions and predictive accuracy of the non-spatial model to one of the spatial models to assess the broader benefits of including spatial information when estimating trends.

We limited all but one of our analyses to a 15-year period, which we considered short enough that a log-linear slope can be a meaningful summary of the population change (Buckland et al. 2004, Thompson and La Sorte 2008). In effect, 15 years is likely long enough to estimate a meaningful rate of change on each route but also short enough to reduce the likelihood of complex non-linear population patterns. The only exception is the Horned Grebe covariate example, where we used a 43-year period because the covariate was designed to adjust for annual fluctuations and non-linear patterns in regional moisture/drought cycles (details below). This 15-year period that we demonstrate here is somewhat arbitrary and for many species

or ecological questions, it may be very informative to fit these models (or modifications of these models) to a longer (or even shorter) period of time.

Model structure

The four models are relatively simple, hierarchical log-link negative binomial regressions, broadly similar to other models commonly applied to the BBS (Sauer and Link 2011, Smith et al. 2014), but modeling trend and abundance as spatially varying coefficients (Barnett et al. 2021, Thorson et al. 2023). For all our models, each route has a separate slope and intercept and there are no annual intercepts to model annual or non-linear temporal patterns in population change. Therefore, the interpretation of "trend" in these models is limited to this log-linear slope parameter (i.e., a single mean rate of change over the entire modeled time-series).

We modeled the observed counts ($C_{r,j,t}$) of a given species on route-r, in year-t, by observer-j as realisations of a negative binomial distribution, with mean $\lambda_{r,j,t}$ and inverse dispersion parameter ϕ. The log of the mean ($\lambda_{r,j,t}$) of the negative binomial distribution was modeled as an additive combination of route-level intercepts (α_r), observer-effects (ω_j), a first-year observer-effect ($\eta I[j,t]$), and route-level slope parameters (β_r) for the continuous effect of year (t) centered on the mid-year of the time-series (t_m).

$$C_{r,j,t} = Negative\ Binomial\left(\lambda_{r,j,t}, \phi\right)$$

$$log\left(\lambda_{r,j,t}\right) = \alpha_r + \beta_r * (t - t_m) + \eta I[j,t] + \omega_j$$

For the parameters that were common to all models, we estimated observer effects drawn from a normal distribution with estimated variances ($\omega_j \sim Normal(0, \sigma_\omega)$), the inverse dispersion parameter as the inverse of a half, standard t-distribution with 3 degrees of freedom ($\phi \sim |t(3,0,1)|^{-1}$), and the first-year observer-effect η, as an independent parameter with a weakly informative prior ($\eta \sim Normal(0,1)$). All other parameters were estimated as hierarchical effects, sharing information among routes or among observers. To encourage convergence, we constrained each of the random effects in the model, including the spatial route-level parameters, to sum to zero. These constraints often improved model sampling

efficiency, but they do not affect the interpretation of the final route-level slopes or intercepts. The models here varied only in the estimation of the route-level intercepts and slope terms. Three of the models used spatial information to estimate the intercepts and slopes (i.e., effectively shrinking towards a local mean of neighboring routes), while the fourth model estimated the intercepts and slopes as simple exchangeable random effects (i.e., shrinking towards a global mean of all routes).

To estimate route-level abundance, while accounting for variation among observers, we modeled separate intercepts for routes and observers. Using separate observer and route effects has not been commonly included in hierarchical Bayesian models for the BBS (Sauer and Link 2011, Smith et al. 2014, Link et al. 2020, Edwards and Smith 2021, but see (Betts et al. 2022, Smith et al. 2023). In general, observers and routes are correlated in the BBS dataset, by design as an experimental control for variation among observers (Kendall et al. 1996). However, observers and routes vary in the number of surveys conducted and the database still contains a lot of information on variation among routes and among observers: considering only the years modeled here (2006 – 2021) more than 2/3 of surveys were conducted on routes that have had more than one observer during those 15 years and more than half of surveys were conducted by observers who have surveyed more than one route. Separating observer from route effects is also possible due to the added spatial information included in the route-level intercept estimate, the sum to zero constraints in the model parameterization, the weakly informative priors that constrain parameters to plausible values given the log-link model, and the improved efficiency of the Hamiltonian Monte Carlo (HMC) samplers in Stan (Betancourt 2018, Stan Development Team 2022) over the Markov Chain Monte Carlo (MCMC) samplers in earlier probabilistic programming languages such as JAGS (Plummer 2003). Finally, we also used an informative prior on the standard deviation of the observer effects (σ_ω), and we ensured that all parameters had converged when fitting the models (details below). We used a half-normal prior on the standard deviation among observers, scaled to imply that variation among observers is unlikely to result in variation in mean counts greater than a factor of approximately 6 (i.e., it is very unlikely that a change in observer on a route will result in a sixfold increase, or reduction, in a given

species abundance; $\sigma_\omega \sim |Normal(0,0.3)|$), and that variation among observers is less than variation among routes. We suggest this prior is reasonable given the screening process used to ensure all BBS observers have adequate experience and bird identification skills for the region they are surveying.

Spatial structures

We fit models with two different approaches to account for spatially explicit relationships among routes: 1) an intrinsic Conditional Autoregressive (iCAR) structure that uses a sparse matrix of adjacencies between pairs of routes, treating spatial relationships as a series of discrete neighbors; and 2) an isotropic Gaussian process (GP) model that uses a matrix of Euclidean distances separating the start locations of each BBS route, treating distance between routes as a continuous measure of separation.

We used these two different approaches, because the spatial locations of BBS observations are not perfectly represented by either discrete areas or points in space. It is not obvious whether the iCAR or the GP better reflects reality (Pebesma and Bivand, 2023), because the observations from a given BBS route are collected along a transect that is approximately 40 km long. Both approaches are necessary simplifications of the true spatial processes underlying variation in abundance and trends among the BBS routes. The iCAR approach (also used for the spatial relationships in the BYM model) simplifies the spatial structure by assuming each route represents a discrete area of space (a polygon surrounding the route), but the neighboring routes may be separated by a wide range of distances depending on the spatial distribution and spatial density of those routes. The GP approach simplifies the spatial relationships by assuming each route represents a point in space, but that measure of intervening distance only applies to the distances between the start points of the routes, not to the full transect. As an example of where the two approaches can differ, the GP could consider the abundance or trends of two distant routes as effectively independent, if the distance is large enough relative to the estimated distance decay function. By contrast, the iCAR structure could consider these same two routes as having a very close connection if there were no intervening routes. In some cases, treating two relatively distant routes as close neighbors

may be useful if their relative proximity provides useful information to inform the parameter estimates, but may also introduce error into the estimate of spatial variance (Pebesma and Bivand 2023).

We used a Voronoi tessellation to generate the discrete neighborhood relationships required to support the iCAR model (Ver Hoef et al. 2018, Pebesma and Bivand 2023). iCAR models are often applied to contiguous area-based stratifications, such as regular grids, census regions, or political jurisdictions, which have natural neighborhood relationships defined by their adjacencies (Ver Hoef et al. 2018, Meehan et al. 2019). To generate contiguous discrete spatial units without imposing a regular grid structure, we used a Voronoi tessellation to create contiguous polygons, centered on the start point of each BBS route (Pebesma 2018). We further limited the adjacency matrix to the approximate boundaries of the species' range, by clipping the tessellated surface using the standard BBS analytical strata where the species occurs (province/territories/states intersected with Bird Conservation Regions; Link and Sauer 2002) and a concave polygon surrounding the routes' start locations (concaveman package; Gombin 2023). This clipping ensured that adjacency relationships did not extend beyond the borders of the species' range and allowed the adjacency matrix to respect large-scale, complex range boundaries (e.g., gaps in forest bird ranges created by the great plains). Within the species' range boundaries, routes were considered neighbors if their Voronoi polygons shared a linear segment along a separating boundary (an edge; Figure 1). This approach to generating these adjacency relationships distorts Euclidian space to create a matrix of relative spatial relationships, because some neighboring routes may be much further apart than others. However, it is sufficiently flexible to ensure a comprehensive and contiguous network of among-route links, and accurately represents those relative spatial adjacencies (each route is considered adjacent to its nearest neighbors). We separately modeled the spatial dependence of intercept parameters (route mean relative abundance) and slope parameters (route trends), under the assumption that each parameter may be influenced by different ecological processes acting at different spatial scales. To fit the GP model, we used a squared exponential kernel to model the isotropic distance-based decline in covariance, assuming that the covariance declines exponentially in all directions, with the squared

distance between the start points of each BBS route. We adapted functions and code in the Stan probabilistic programming language from the "rethinking" R-package for inclusion in our GP model (McElreath 2023). Similar to the iCAR approach, we used independent GPs to model the covariance of the intercept parameters and the slope parameters. We estimated the full matrix for between-route distances using functions in the "sf" package for R (Pebesma 2018).

Intrinsic Conditional Autoregressive model - iCAR

We estimated the route-level intercepts and slopes using an iCAR structure, where the parameter for route-r is drawn from a normal distribution, centered on the mean of that parameter's values in all neighboring routes, with an estimated standard deviation that is proportional to the inverse of the number of neighbors for that route (Morris et al. 2019). Specifically, the intercept term that represents the mean relative abundance on each route (α_r) is estimated as an additive combination of a species-mean (α'_r) and a random route-level term (α''_r) drawn from a normal distribution centered on the mean of the intercepts for all neighboring routes ($\alpha_r = \alpha' + \alpha''_r$).

$$\alpha''_r \sim Normal\left(\frac{\sum_{n \in N_r} \alpha''_n}{N_r}, \frac{\sigma_{\alpha''}}{N_r}\right)$$

The slopes representing the trend on each route (β_r) were estimated similarly as a species-level mean trend plus random route-level terms from a normal distribution centered on the mean of the slopes for all neighboring routes ($\beta_r = \beta' + \beta''_r$).

$$\beta''_r \sim Normal\left(\frac{\sum_{n \in N_r} \beta''_n}{N_r}, \frac{\sigma_{\beta''}}{N_r}\right)$$

Besag York Mollie iCAR model - BYM

We used an implementation of the Besag, York, Mollié (BYM) spatial iCAR model (Besag et al. 1991) to estimate route-level slopes. This model is an elaboration on the iCAR model where we estimated the slopes as additive combinations of a spatial random effect and a non-spatial random effect (Besag et al. 1991).

$$\beta_r = \beta' + \beta''_{space_r} + \beta''_{non-space_r}$$

We estimated the spatial component using the same structure as for the iCAR model.

$$\beta''_{space_r} \sim Normal\left(\frac{\sum_{n \in N_r} \beta''_{space_n}}{N_r}, \frac{\sigma_{\beta_{space}}}{N_r}\right)$$

We estimated the additional non-spatial component as a simple random effect drawn from a normal distribution with an estimated standard deviation:

$$\beta''_{non-space_r} \sim Normal\left(0, \sigma_{\beta_{non-space}}\right)$$

The additional random effect included in the BYM model, allowing the route-level trend estimates to vary more among neighboring routes, if supported by the data (Besag et al. 1991).

Gaussian Process model - GP

In the Gaussian Process (GP) model, the intercepts and slopes were also estimated as the sum of a route-level random term and a species-level mean ($\beta_r = \beta' + \beta''_r$). The slope and intercept random terms for each route (β''_r and α''_r) are estimated as zero-mean, multivariate normal distributions, $\beta'' \sim MultivariateNormal(0, K_\beta)$ and $\alpha'' \sim MultivariateNormal(0, K_\alpha)$,with covariance matrices (K_β and K_α) estimated using a squared exponential kernel function (Gelman et al. 2013, pg 501). The covariance of the slope parameters for two routes ($k_\beta(\beta''_1, \beta''_2)$) is a function of the distance between them ($d_{1,2}$) plus the two parameters that control the magnitude of the covariance when distance is zero (θ_β) and the scale of the spatial dependency (ρ_β).

$$k_\beta(\beta_1'', \beta_2'') = \theta_\beta^2 * e^{\left(-\rho_\beta^2 * d_{1,2}^2\right)}$$

We estimated the intercept parameters using the same squared exponential kernel function with separate parameters for the magnitude and scale of the spatial dependency.

$$k_\alpha(\alpha_1'', \alpha_2'') = \theta_\alpha^2 * e^{\left(-\rho_\alpha^2 * d_{1,2}^2\right)}$$

The parameters of GP models can be quite sensitive to prior distributions (McElreath 2020). We scaled the distance matrix in units of 1000 km and set a half-standard t-distribution prior on θ_α^2 and θ_β^2 with 5 degrees of freedom (Gelman et al. 2013). The half-t prior on θ^2 places most prior mass at relatively small values and includes a relatively long tail that allows for larger values, if supported by the data. For most species, we used a weakly informative, inverse gamma distribution prior with scale and shape = 5 for ρ_α^2 and ρ_β^2. For some species, the values of ρ^2 failed to converge with this prior, so we set an alternative and more informative prior using a gamma distribution with scale and shape = 2. The gamma and inverse gamma priors on ρ^2 both avoid 0, ensuring that spatial dependency decreases with distance. The weakly informative inverse gamma includes a long right tail that allows the model to estimate spatial dependency that declines steeply with distance (e.g., $\rho_\alpha^2 > 500$ and therefore covariance values near 0 for routes separated by the approximate 40-km length of a BBS route), but for some species this long tail created convergence difficulties. For these species, we used the gamma prior with a shorter right tail and effectively constrained the estimates of ρ^2 to values < 20. This places most of the prior mass at values that imply there is some spatial dependency that may extend out to larger distances (500 km – 3000 km).

Non-spatial model

To assess the benefits of assuming spatial dependence among BBS routes, we compared the predictions and predictive accuracy of the spatial models to an otherwise identical model that lacked spatial information. This non-spatial model had all the same parameters as the spatial models, except that the route-level intercepts and slopes were estimated as simple random effects.

$$\beta_r'' \sim N\left(0, \sigma_{\beta_{non-space}}^2\right)$$

$$\alpha_r'' \sim N\left(0, \sigma^2_{\alpha_{non-space}}\right)$$

Remaining priors

We used weakly informative (Gelman 2006, Lemoine 2019), standard normal priors for the mean species-level intercept and the first-year effect parameter. The mean species-level slope parameter was given a weakly informative normal prior ($\beta' \sim Normal(0, 0.1)$). We consider this prior weakly informative as it reflects our belief that extreme rates of change are unlikely (it places approximately 95% of the prior mass for the survey-wide population trends between -20 and +20%/year).

For the iCAR, BYM, and non-spatial models, the priors for the standard deviations of the spatial variation and non-spatial variation of the route-level slopes ($\sigma_{\beta_{spatial}}$ and $\sigma_{\beta_{non-space}}$) had gamma priors with shape = 3 and scale = 30. These gamma priors were weakly informative such that the standard deviation of trends was constrained to more probable scales based on the log-link of the model and to avoid estimates of zero (Chung et al. 2013). Specifically, this gamma prior places the mean of the prior mass at approximately 10% per year, and 99% of the prior mass on the standard deviation of route-level trends at values less than 28% per year, while also including a long tail so that the model can estimate more extreme variation if supported by the data (Chung et al. 2013). The standard deviation of the intercept terms in these models ($\sigma_{\alpha_{spatial}}$ and $\sigma_{\alpha_{non-space}}$) were given a half-normal prior with standard deviation = 2. This weakly informative prior places most prior mass at values < 5, and reflects our belief that across a species' range, mean relative abundance can vary a great deal but is unlikely to vary by more than a few orders of magnitude. For some species, this relatively wide prior created convergence issues, so for these species we re-fit the models with a prior that considered the observed variation in mean counts among routes for a given species. Specifically, we used a half-normal prior with the standard deviation equal to the observed standard deviation of mean log-transformed observed counts among routes. We are confident that this prior is only weakly informative and likely over-estimates the among-route variance because the observed data includes variation among routes as well as variation among observers.

Convergence

We fit all models using 1000-2000 warmup iterations and an equal number of sampling iterations for each of the 4 independent chains (or 3 independent chains for each iteration of cross-validation). We assessed convergence by monitoring for divergent transitions and estimating split-Rhat values and bulk effective sample sizes for all parameters. We considered convergence to have failed if any Rhat was greater than 1.03 or if any parameter's effective sample size was < 100 (although the vast majority of parameters had effective sample sizes > 1000 and Rhat < 1.01). If any models did fail to converge, we re-fit the models with the alternative priors described above.

Model assessment

To assess the benefits of adding spatial information into the model, we compared the 1-step-ahead, leave-future-out (LFO) predictive success of the four models for the 71 species with relatively small ranges (Roberts et al. 2017, Bürkner et al. 2020). We also ran a LFO assessment comparing the iCAR spatial model with the non-spatial version of the model for the remaining 216 species (Table 1). We used the LFO approach to directly test the temporal predictions of the models (i.e. test the accuracy of predictions of next year's observations). In this application of LFO, we fit the model to the first 8 years of data (2006-2013; the minimum length of time we considered sufficient for prediction), and used the parameter estimates from this model to predict the counts in the following year (2014). Then we iterated this approach making predictions for the remaining years (2015-2019, and 2021), predicting the observed data in year n using data for all years up to year(n-1) to fit the model. We could not assess predictive accuracy for the year 2020, because the BBS was cancelled due to concerns over COVID-19. The cross-validation process generated predictions for every count in the dataset, and an estimate of the log pointwise predictive density (lppd) of the observed count, given the model and the data in all previous years (Gelman et al. 2014). For interpretation and visualization, we calculated pairwise differences in lppd between pairs of models for each count and transformed summaries of these lppd-differences across many counts into the approximate z-scores used (Link and Sauer 2016); this provided an interpretable and consistent scale to summarize pair-wise model comparisons across species.

Route-level covariate examples

Modeling covariates of finer-scale trends and relative abundances is a major benefit of modeling BBS trends and abundances at the route-level. To demonstrate this, we present two examples, each including route-level predictors to inform estimates of abundance and trend. The first example uses data on the Rufous Hummingbird (*Selasphorus rufus*) and models the effect of habitat suitability on relative abundance and trend. The second example looks at the effects of annual variation in available habitat—the number of ponds surrounding a BBS route in a given year in the Prairie Pothole region (PPR)—on the expected counts of a water bird, the Horned Grebe (*Podiceps auratus*).

Rufous Hummingbird covariate example

This example application is an elaboration of the iCAR route-level trend model, where the route-level intercepts and slopes are additive combinations of two components: 1) one that is a function of a route-level predictor, and 2) one that is a residual component, estimated using the iCAR structure (Ver Hoef et al. 2018). The route-level predictors are derived from a previous study on Rufous Hummingbirds that modeled variation in habitat suitability over space and time (Jefferys et al. unpublished, supplemental methods). Mean habitat suitability for a given year within a 200m buffer of each BBS route was used as a predictor on the intercept (i.e., the mean relative abundance on a given route). The rate of change in habitat suitability over time within the same buffer was used as a predictor on the slope (i.e., the trend in the species' abundance). This model structure relies on relatively simple assumptions that the amount of habitat around a BBS route should predict the mean number of birds observed, and that the change in habitat amount should predict the change in the number of birds.

We estimated the route-level intercepts and slopes as an additive combination of a mean species-level intercept or slope (α' or β'), a varying intercept or slope that was a function of the mean habitat suitability on the route (α_r''') or rate of change in habitat suitability on the slope (β_r'''), and spatially varying effects for the residual variation in relative abundance (α_r'') and slope (β_r'') that were not explained by habitat.

$$\alpha_r = \alpha' + \alpha_r'' + \alpha_r'''$$

$$\beta_r = \beta' + \beta_r'' + \beta_r'''$$

This partitioning of the intercept and slope parameters allows the model to generate two alternative estimates of the mean abundance and trend on each route. The full trend ($\beta' + \beta_r'' + \beta_r'''$) represents the full estimated trend on a given route, including the effects of habitat change. The residual trend ($\beta' + \beta_r''$) represents an alternate trend if the habitat had stayed constant on a given route. Similarly, the full relative abundance ($\alpha' + \alpha_r'' + \alpha_r'''$) represents the full estimated relative abundance on a given route, including the effects of habitat. The residual relative abundance ($\alpha' + \alpha_r''$) represents an alternate abundance that would have been expected if the habitat suitability were the same across all routes.

We estimated the effect of mean habitat suitability on the route-level intercept as a simple product of a route-specific coefficient (ρ_{α_r}) and mean (across all years; 2006-2021) habitat suitability in a 200m buffer around each route-path ($\alpha_r''' = \rho_{\alpha_r} * MeanSuitability_r$). To model the effects of habitat change on population trend, we estimated the effect of the rate of change in habitat suitability on each route ($ChangeSuitability_r$) with a route-specific coefficient (ρ_{β_r}). The route-specific coefficients for the effects of habitat suitability on the intercept and slope were allowed to vary among routes, but were centered on hyperparameter mean effects across routes $\rho_{\alpha_r} \sim Normal(P_\alpha, \sigma_{\rho_\alpha})$ and $\rho_{\beta_r} \sim Normal\left(P_\beta, \sigma_{\rho_\beta}\right)$. As such, the hyperparameters for the effect of mean habitat suitability on the intercept (P_α) and the effect of change in habitat suitability on slope (P_β) represent a clear species-level estimate of the overall effects of habitat on abundance and trend, after adjusting for the residual, spatially-dependent variation in abundance and trend.

Horned Grebe covariate example

This example application is an elaboration of the iCAR route-level trend model, where trends and relative abundances are estimated while accounting for the annual variation in climatically dependent habitat. The route-level predictors are derived from a study of the effects of moisture/drought patterns on Horned

418 Grebe (supplemental methods), a waterbird species which breeds in small to moderately sized shallow
419 freshwater ponds (Stedman 2020). To represent annual variation in available habitat for the Horned Grebe
420 in the Canadian Prairie Pot Holes Region (PPR), we used data collected by the U.S. Fish and Wildlife
421 Service (USFWS) and the Canadian Wildlife Service (CWS) on the number of ponds (natural or artificial
422 ponds that are flooded seasonally, semi-permanently and permanently) during the Waterfowl Breeding
423 Population and Habitat Survey (U.S. Fish and Wildlife Service 2022). Annual fluctuations in moisture
424 affect the number of wetlands available, which has a strong influence on waterbird populations that are
425 highly dependent on wetlands abundance (Sorenson et al. 1998, Johnson et al. 2005, Roy 2015, Steen et
426 al. 2016). The model uses the iCAR model and adds an additional iCAR component to create a varying-
427 coefficient model on the effects of available habitat on the observed counts during a given survey on a
428 given route.
429
430 We estimated the effect of the number of ponds in a buffer surrounding BBS routes as a spatially-varying
431 coefficient representing the route-specific effect of local ponds ($\rho_r * ponds_{r,t}$). Local ponds are the
432 number of ponds surrounding a BBS route each year, where $ponds_{r,t}$ represents the log(1 + number of
433 ponds) surrounding BBS route r in year t, centered on the mean number of ponds across years for each
434 route. This route-specific centering ensured we could separately estimate the route-level intercepts and the
435 effects of the annual variations in ponds and ensured that it only represented the temporal variation in
436 ponds and not the spatial variation. The effects of ponds per route were centered on a mean
437 hyperparameter (ρ_r') and allowed to vary among routes using the same iCAR spatial structure as for the
438 slopes and intercepts (ρ_r'').

439 $$\rho_r = \rho_r' + \rho_r''$$

440 $$\rho_r'' \sim Normal\left(\frac{\sum_{n \epsilon N_r} p_n''}{N_r}, \frac{\sigma_{p''}}{N_r}\right)$$

Finally, we also fit the same data to the simple iCAR model (i.e., an identical model with no covariates) to compare the difference in estimated trends with and without accounting for the annual variations in available habitat.

Results

In general, there are clear spatial patterns in the estimated trends and relative abundances from the spatial models, the patterns are similar among the three types of spatial models, and those patterns are obscured or completely lacking from the non-spatial version of the model (e.g., the results for Baird's Sparrow in Figures 2 and 3). The GP model tended to smooth the spatial pattern in trends more than the iCAR model, which in turn smoothed more than the BYM model (Figure 2). The spatial smoothing in relative abundance was stronger in both the iCAR and BYM models than the GP model for Baird's Sparrow (Figure 2. The covariance in relative abundance of Baird's Sparrow among routes was effectively 0 at distances of only 100 km (posterior mean of ρ_{α}^{2} = 650), whereas the covariance in trend was relatively strong even at distances > 1000 km (posterior mean of ρ_{β}^{2} = 1.5, Figure S1). Predictions of route-level trends had smaller standard errors when including spatial information, and trend precision generally increased with the degree of spatial smoothing (Figure S2). For Baird's Sparrow, all three spatial models had better predictive accuracy than the non-spatial model, with z-scores of pairwise differences between one of the spatial models and the non-spatial model ranging from 2.7 – 3.3 (Figure S4). The iCAR model had better predictive accuracy than the BYM model (z-score of the difference = 3.8, Figure 4), and there was little difference in predictive accuracy between the iCAR and GP models (z-score difference = -0.51, Figure 4).

The leave future out (LFO) cross-validation shows that the iCAR and GP models out-perform the non-spatial model (more accurately predicted next-year's data), for almost all the 71 small-range species (Figure 4 and Figure S4). The BYM model had lower predictive accuracy than the other spatial models. It had lower accuracy than the iCAR model for all species and was the only spatial model that had clearly lower predictive accuracy than the non-spatial model (i.e., four species for which the z-score difference is < -2, Figure 4 and Figure S4). The iCAR model and the GP model had similar predictive accuracy for many species; just over 2/3 of the species were better predicted by the GP model (49 of 71 species) and the remaining species were better predicted by the iCAR model (Figure 4). When including the additional

216 species for which fitting the GP model was prohibitively time-consuming (days or even weeks required for convergence for a given species), the iCAR model had higher predictive accuracy than the non-spatial model for 283 of 287 species, and predictive accuracy was very similar for the remaining four (Figure 5).

The iCAR model generated trend prediction maps with clear spatial patterns that likely relate to spatially dependent variation in processes affecting populations (Figure 6). These patterns are not evident in predictions from an identical model without spatial information (Figure 6). The spatial patterns in route-level trends vary widely among species (Figures S4 and S5), suggesting varied drivers of population change across the continent and among species.

In general, the iCAR and GP models were comparable in predictive accuracy for the 71 small-range species we analyzed (Figure S9). In addition, the spatial patterns in predicted trends were very similar between these two models, even for species where the predictive accuracy differed between the models. For example, the GP model had higher predictive accuracy than the iCAR model (z-score difference = -4.3) for Canyon Towhee (*Melozone fusca*), but the opposite was true for Western Bluebird (*Sialia mexicana*; z-score difference = 2.3, Figure S4). Regardless, the spatial pattern in predicted trends between the two models is quite similar for both species (Figure 7). For both species, and in general, the GP model trend estimates had narrower credible intervals (higher estimated precision) than the iCAR model (Figure S6). Precision of the iCAR trend estimates also showed a clear relationship to the number of neighbors for any given route, in that routes with few neighbors (on the edges of the species' range) were much less precise than estimates in the core of the species' range (Figure S6).

Including habitat suitability in the Rufous Hummingbird population model had an effect on estimates of route-level abundance and improved estimates of the spatial pattern in long-term trends, however much of the overall decline was not related to route-level habitat-change (Figure 8). The effect of habitat suitability on mean relative abundance was strong and positive (P_{α} = 3 [95% CI 2.2:3.8]), such that routes with higher overall habitat suitability had higher mean counts. From 2006-2021, the Rufous

Hummingbird's overall population declined steeply, decreasing by approximately -43% (95% CI -52:-33) over the 15 years. There was an effect of change in habitat suitability on trends, such that routes with habitat loss had more negative population trends P_{β} = 0.025 95% CI 0.003:0.047. Trends were negative across the species' range, but most negative in the coastal regions where the habitat has changed the most and where the species is also most abundant (left panel, Figure 8). The change in habitat suitability affected the spatial patterns in trend (Figure 8), the greater loss of habitat in the coastal regions (Figure S7) accounts for most of the increased rates of decline in the core of the species' range, the residual trend component alone does not show the same coastal-decline pattern (Figure 8, right panel). However, changes in habitat suitability did not account for the overall decline in the species population, as the data suggest negative population trends across the species' range after removing the effects of local habitat change (right-panel in Figure 8).

Annual variation in the number of ponds around BBS routes affected the overall rate of population change in Horned Grebes and showed a spatial relationship (Figure 9). In a model including the annual pond variation, the Horned Grebe population declined overall at a rate of -1.9 %/year from 1975-2017. After removing the effect of annual pond variation, the long-term rate of decline was -2.2 %/year. The effect of annual fluctuations in the number of ponds was positive across the region: the mean value of P = 0.42 95% CI 0.29:0.55, but there was also a spatial gradient in intensity. The effect of the number of ponds per year was strongest in the northwest part of the Prairies (Figure 9) and declined to the south and the east.

Discussion

Spatially explicit, route-level models are useful for visualizing fine spatial patterns at scales more relevant to local conservation, understanding the drivers of population change, and estimating the effects of covariates on relative abundance and trends (e.g., Betts et al. 2022). At this fine spatial scale, incorporating spatial information improved the models' predictions of future data. This improvement was particularly clear for both the iCAR and the GP models, where these spatial models had higher accuracy for out-of-sample predictions than the non-spatial model for almost every species compared. The spatial patterns in trend estimates should be useful for visualizing the variations in trends across the species' range that may help generate hypotheses of the ecological drivers of population change and potential conservation strategies. Route-level models also allow for the incorporation of local habitat covariates on abundance and trend at fine scales, which is important as some covariates affect bird populations at scales much smaller than strata often used for broad-scale analyses, such as Bird Conservation Regions (BCRs) or states/provinces (Thogmartin et al. 2004, Paton et al. 2019, Monroe et al. 2022). Route-level patterns are useful in guiding conservation and/or further monitoring efforts, such as identifying small areas for conservation purposes or diverging population trends within management areas (i.e., strata or BCR).

These route-level, spatial models generate smoothed patterns of variation in population trends across a species' range which will greatly facilitate the hypothesis generation and direct investigation to better understand the drivers of population change, similar to (Fink et al. 2023). For example, the spatial models show relatively smooth patterns in Baird's Sparrow trends across the species' range (Figure 2), which are not evident in the simpler, non-spatial model. In the spatial models, the Baird's Sparrow has increased in the west and decreased in the eastern portions of its range. This latitudinal pattern may suggest hypotheses related to spatial variation in factors related to weather or climate, which could then be directly tested by incorporating covariates representing these factors into a subsequent model. Similarly, the complex spatial patterns in the trends of Hairy Woodpecker (*Dryobates villosus*, Figure 6) show some latitudinal variation in trends in the west that is not as clear in the East, suggesting that there may be distinct processes driving trends in these two regions. Comparisons of these patterns among species may

be particularly informative. For example, the somewhat similar southeast to northwest gradients in trends for Canyon Towhee and Western Bluebird may suggest some similarity in the underlying drivers (Figure 7). These are only speculations, and simply provide examples of the kinds of hypothesis generating explorations that are facilitated by these fine-scale, spatially explicit models of structured monitoring data.

All three of the spatial models (iCAR, GP, and BYM) generated broadly similar spatial patterns in route-level trends for the subset of species we compared (Figure 4 and Figure S3). The best spatial structure to use will depend on the species and the goals of a particular study. For the species here, there was little support for the extra variation in route-level trends in the BYM model; it had lower predictive accuracy than the simpler iCAR model in all cases. The iCAR structure outperformed the GP models for 1/3 of the species here, and it is more computationally efficient. Overall, the GP model outperformed the iCAR model for most (2/3) of the species compared here. In general, the GP model also estimated smoother spatial patterns in population trends than the other spatial models and for some the difference is striking (e.g., Black−throated Gray Warbler, *Setophaga nigrescens*, California Quail, *Callipepla californica,* and Golden−winged Warbler, *Vermivora chrysoptera* in Figure S3). For the first two species the GP outperformed the iCAR for accuracy, while for the third species, the iCAR was better (Figure S4). Additionally, although the GP parameterization that we used here required significantly more computational effort, more efficient ways of implementing Bayesian GP models are being developed (Hoffmann and Onnela 2023). For larger datasets (e.g., broad-ranging species and or longer time-series), the iCAR structure may be preferable simply for speed. Since there are many ways to define neighborhood relationships (Freni-Sterrantino et al. 2018), it may provide more direct control to model discontinuities in the spatial relationships, such as complex range boundaries (Ver Hoef et al. 2018, Pebesma and Bivand 2023). A species with limited dispersal may be particularly sensitive to the Euclidean distance between points and therefore better modeled with the GP, but the simplification of space using the iCAR structure may be sufficient for most wide-ranging migratory birds. For example, for

some species there are routes on the periphery of the BBS sampling distribution or the periphery of a species' range that are separated from most other routes by relatively large distances. These "isolated" routes are treated very differently by the iCAR and GP models; they are considered close neighbors in the iCAR model irrespective of the intervening distance, whereas, in the GP model, the large separation from other routes reduces their correlation with their nearest neighbors. Interestingly, when we compared the predictive accuracy between GP and iCAR models for routes that were more isolated than most (nearest neighboring route > 200km away), the simplified relative-spatial relationships of the iCAR tended to outperform the continuous spatial treatment of the GP for these isolate routes (Figure S8). Therefore, although the more accurate representation of the long distances separating these isolated routes in the GP model does not necessarily result in more accurate predictions.

These route-level BBS models provide many opportunities for further applications, elaborations with covariates, and comparisons to other sources of trend information. The fine-scale estimates could be summarized across species and within regions, such as summaries of the spatial patterns in grassland bird trends or summaries for a given species within BCRs or states/provinces and compared to estimates from models fit at those broader spatial scales. The spatial patterns in trend estimates also allow for comparison of BBS data to other fine-grained maps of species trend and relative abundance, such as eBird (Sullivan et al. 2014, Fink et al. 2023) or the Integrated Monitoring in Bird Conservation Regions (IMBCR) program (Pavlacky et al. 2017). Comparison of trend estimates between the two programs for the same species and periods of time could provide useful validation of and or help understand differences between the two sources of information. Similarly, there are many possible avenues to integrate information across programs for a given period (e.g., recent trends) or through time (e.g., long-term information from the BBS with more recent information from eBird and/or IMBCR). We see an almost limitless potential for customizing route-level BBS models to include covariates testing hypotheses of drivers of population abundance and trends (e.g., Betts et al. 2023). The examples of covariate models here and our application

of LFO cross-validation will hopefully provide useful tools to better understand the causes of population change in North American birds.

Separating the route-level intercepts from the observer-level intercepts allowed us to better model patterns in relative abundance. It should also allow for improved modeling of among observer variation. Although many previous BBS analyses have treated each observer-route combination as an independent sampling unit (Link et al. 2020, Smith and Edwards 2020), doing so necessarily allocates some of the biological variation in abundance in space (i.e., among-route variation in abundance) to an effect that is treated as sampling noise (among-observer variation). The model will struggle to separately estimate intercepts for observers and routes in situations where there are few data to inform the estimates (e.g., intercepts for observers who only contribute data to a route that has never been surveyed by another observer). However, we suggest that a model that includes a few of these weakly estimable parameters is likely preferable to a model that fails to attempt to separate the biological variation among routes from the sampling noise of observer variation, at least in the situations where there are data to support their separation. In a practical sense, this separation of the observer from route effects is improved by the hierarchical structure of the models, spatial information, weakly informative priors and the improved efficiency of HMC algorithms over the Gibbs sampling algorithms of earlier Bayesian BBS models. Although initially motivated by our desire to directly model route-level abundance, this approach is equally applicable to other BBS analyses (Smith et al. 2023), and is included in the models in the R-package bbsBayes2 (Edwards et al. 2023).

In our covariate examples, not only did we estimate local effects of covariates on abundance and trend, but covariates revealed important spatial patterns. For the Rufous Hummingbird, the model showed higher mean abundance on routes with more habitat and positive effects of the change in habitat on the species' trend (more negative trends on routes where habitat has decreased). Interestingly, it also showed that during this period, the variation among routes in habitat change does not account for all of the decline in the species population (Figure 8, and Figure S7), suggesting that factors other than local habitat or

624 acting outside of the breeding range may be driving the overall decline. For the Horned Grebe, the effect
625 of annual fluctuations in available wetland habitat (the number of ponds) was positive overall and also
626 varied in magnitude across the species' range. The effect was strongest in the western prairies where the
627 effects of drought are often strongest (Millett et al. 2009, Johnson et al. 2010, Roy 2015). These results
628 highlight that waterbird populations breeding in the Prairie Potholes Region remain vulnerable to habitat
629 modifications and climate change, but also suggest strategies and conservation actions in regions where
630 the waterbird species are the most vulnerable. In both examples, the ability to incorporate spatial
631 covariates into the trend analysis tested hypotheses around the drivers of population change and helped to
632 identify specific areas for further research and conservation action.

633 Finer-scale estimates can be used to inform finer-scale municipal and community-level decisions and to
634 communicate science at a level important to both communities and volunteers. Decisions on
635 anthropogenic land use change for industries such as agriculture, forestry, and housing are often made at
636 fine scales (Sodhi et al. 2011, Malek et al. 2019). Likewise, habitat protection and restoration by
637 community organizations, municipal governments, and NGOs occur at fine scales (Sheppard 2005,
638 Aronson et al. 2017). For example, the Horned Grebe covariate analysis confirmed the vulnerability of
639 waterbird species in the northwestern Prairie Potholes Region and supported a current initiative to protect
640 critical shallow wetlands in the region (Prairie Habitat Joint Venture 2020). Community support is
641 important for the success of conservation initiatives (Berkes 2004, Bennett and Dearden 2014), providing
642 estimates at scales relevant to communities may increase community support for conservation and
643 encourage a feeling of stewardship. Further, the routes are a relevant scale for the dedicated BBS
644 volunteers, with the average BBS volunteer participating for 12 years. Producing estimates at a route-
645 level provides a tangible outcome of volunteers' efforts and would allow them to share their direct
646 contributions, a large motivator for many citizen science volunteers (Phillips et al. 2019).

647

References Cited

Aronson, M. F., C. A. Lepczyk, K. L. Evans, M. A. Goddard, S. B. Lerman, J. S. MacIvor, C. H. Nilon, and T. Vargo (2017). Biodiversity in the city: key challenges for urban green space management. Frontiers in Ecology and the Environment 15:189–196.

Barnett, L. A. K., E. J. Ward, and S. C. Anderson (2021). Improving estimates of species distribution change by incorporating local trends. Ecography 44:427–439.

Bennett, N. J., and P. Dearden (2014). Why local people do not support conservation: Community perceptions of marine protected area livelihood impacts, governance and management in Thailand. Marine Policy 44:107–116.

Berkes, F. (2004). Rethinking Community-Based Conservation. Conservation Biology 18:621–630.

Besag, J., J. York, and A. Mollié (1991). Bayesian image restoration, with two applications in spatial statistics. Annals of the Institute of Statistical Mathematics 43:1–20.

Betts, M. G., Z. Yang, A. S. Hadley, A. C. Smith, J. S. Rousseau, J. M. Northrup, J. J. Nocera, N. Gorelick, and B. D. Gerber (2022). Forest degradation drives widespread avian habitat and population declines. Nature Ecology & Evolution 6:709–719.

Drever, M. C., A. C. Smith, L. A. Venier, D. J. H. Sleep, and D. A. MacLean (2018). Cross-scale effects of spruce budworm outbreaks on boreal warblers in eastern Canada. Ecology and Evolution 8:7334–7345.

Edwards, B. P. M., A. C. Smith, and S. LaZerte (2023). bbsBayes2. [Online.] Available at https://github.com/bbsBayes/bbsBayes2.

Fink, D., A. Johnston, M. Strimas-Mackey, T. Auer, W. M. Hochachka, S. Ligocki, L. Oldham Jaromczyk, O. Robinson, C. Wood, S. Kelling, and A. D. Rodewald (2023). A Double machine learning trend model for citizen science data. Methods in Ecology and Evolution 14:2435–2448.

Freni-Sterrantino, A., M. Ventrucci, and H. Rue (2018). A note on intrinsic conditional autoregressive models for disconnected graphs. Spatial and Spatio-temporal Epidemiology 26:25–34.

Golding, N., and B. V. Purse (2016). Fast and flexible Bayesian species distribution modelling using Gaussian processes. Methods in Ecology and Evolution 7:598–608.

Government of Canada (2010). Cosewic / Cosepac - Definitions associated with quantitative criteria. [Online.] Available at https://www.cosewic.ca/index.php/en-ca/assessment-process/wildlife-species-assessment-process-categories-guidelines/quantitative-criteria-definitions.html.

Hoffmann, T., and J.-P. Onnela (2023). Scalable Gaussian Process Inference with Stan. [Online.] Available at http://arxiv.org/abs/2301.08836.

Hudson, M.-A. R., C. M. Francis, K. J. Campbell, C. M. Downes, A. C. Smith, and K. L. Pardieck (2017). The role of the North American Breeding Bird Survey in conservation. The Condor 119:526–545.

IUCN (2012). IUCN Red List Categories and Criteria: Version 3.1. 2nd edition. IUCN, Gland, Switzerland and Cambridge, UK.

Johnson, W. C., B. V. Millett, T. Gilmanov, R. A. Voldseth, G. R. Guntenspergen, and D. E. Naugle (2005). Vulnerability of Northern Prairie Wetlands to Climate Change. BioScience 55:863–872.

Johnson, W. C., B. Werner, G. R. Guntenspergen, R. A. Voldseth, B. Millett, D. E. Naugle, M. Tulbure, R. W. H. Carroll, J. Tracy, and C. Olawsky (2010). Prairie Wetland Complexes as Landscape Functional Units in a Changing Climate. BioScience 60:128–140.

Link, W. A., J. R. Sauer, and D. K. Niven (2020). Model selection for the North American Breeding Bird Survey. Ecological Applications 30:e02137.

Malek, Ž., B. Douw, J. V. Vliet, E. H. V. D. Zanden, and P. H. Verburg (2019). Local land-use decision-making in a global context. Environmental Research Letters 14:083006.

Meehan, T. D., N. L. Michel, and H. Rue (2019). Spatial modeling of Audubon Christmas Bird Counts reveals fine-scale patterns and drivers of relative abundance trends. Ecosphere 10:e02707.

Millett, B., W. C. Johnson, and G. Guntenspergen (2009). Climate trends of the North American prairie pothole region 1906–2000. Climatic Change 93:243–267.

Monroe, A. P., J. A. Heinrichs, A. L. Whipple, M. S. O'Donnell, D. R. Edmunds, and C. L. Aldridge (2022). Spatial scale selection for informing species conservation in a changing landscape. Ecosphere 13:e4320.

Morrison, C. A., R. A. Robinson, J. A. Clark, and J. A. Gill (2010). Spatial and temporal variation in population trends in a long-distance migratory bird. Diversity and Distributions 16:620–627.

North American Bird Conservation Initiative (2022). The State of the Birds, United States of America.

North American Bird Conservation Initiative Canada (2019). The State of Canada's Birds, 2019. Environment and Climate Change Canada.

Paton, G. D., A. V. Shoffner, A. M. Wilson, and S. A. Gagné (2019). The traits that predict the magnitude and spatial scale of forest bird responses to urbanization intensity. PLOS ONE 14:e0220120.

Pavlacky, D. C., P. M. Lukacs, J. A. Blakesley, R. C. Skorkowsky, D. S. Klute, B. A. Hahn, V. J. Dreitz, T. L. George, and D. J. Hanni (2017). A statistically rigorous sampling design to integrate avian monitoring and management within Bird Conservation Regions. PLOS ONE 12:e0185924.

Pebesma, E., and R. Bivand (2023). Spatial Data Science: With Applications in R. 1st edition. Chapman and Hall/CRC, Boca Raton.

Phillips, T. B., H. L. Ballard, B. V. Lewenstein, and R. Bonney (2019). Engagement in science through citizen science: Moving beyond data collection. Science Education 103:665–690.

Prairie Habitat Joint Venture (2020). Prairie Habitat Joint Venture: The Prairie Parklands Implemenetation Plan 2013-2020. [Online.] Available at https://www.phjv.ca/wp-content/uploads/2020/12/PHJV-Implemenetation-Plan-PRAIRIE-PARKLAND-2013-2020-Final.pdf#page=33.

Renfrew, R. B., D. Kim, N. Perlut, J. Smith, J. Fox, and P. P. Marra (2013). Phenological matching across hemispheres in a long-distance migratory bird. Diversity and Distributions 19:1008–1019.

Rosenberg, K. V., P. J. Blancher, J. C. Stanton, and A. O. Panjabi (2017). Use of North American Breeding Bird Survey data in avian conservation assessments. The Condor 119:594–606.

Rosenberg, K. V., A. M. Dokter, P. J. Blancher, J. R. Sauer, A. C. Smith, P. A. Smith, J. C. Stanton, A. Panjabi, L. Helft, M. Parr, and P. P. Marra (2019). Decline of the North American avifauna. Science 366:120–124.

Roy, C. (2015). Quantifying Geographic Variation in the Climatic Drivers of Midcontinent Wetlands with a Spatially Varying Coefficient Model. PLOS ONE 10:e0126961.

Sauer, J. R., J. E. Fallon, and R. Johnson (2003). Use of North American Breeding Bird Survey Data to Estimate Population Change for Bird Conservation Regions. The Journal of Wildlife Management 67:372–389.

Sauer, J. R., K. L. Pardieck, D. J. Ziolkowski, A. C. Smith, M.-A. R. Hudson, V. Rodriguez, H. Berlanga, D. K. Niven, and W. A. Link (2017). The first 50 years of the North American Breeding Bird Survey. The Condor 119:576–593.

Sheppard, S. R. (2005). Participatory decision support for sustainable forest management: a framework for planning with local communities at the landscape level in Canada. Canadian Journal of Forest Research 35:1515–1526.

Smith, A., A. Binley, L. Daly, B. Edwards, D. Ethier, B. Frei, D. Iles, T. Meehan, N. Michel, and P. Smith (2023). Spatially explicit Bayesian hierarchical models for avian population status and trends. Population Biology.

Smith, A. C., and B. P. M. Edwards (2020). North American Breeding Bird Survey status and trend estimates to inform a wide range of conservation needs, using a flexible Bayesian hierarchical generalized additive model. The Condor. https://doi.org/10.1093/ornithapp/duaa065

Sodhi, N. S., R. Butler, W. F. Laurance, and L. Gibson (2011). Conservation successes at micro-, meso- and macroscales. Trends in Ecology & Evolution 26:585–594.

Sorenson, L. G., R. Goldberg, T. L. Root, and M. G. Anderson (1998). Potential Effects of Global Warming on Waterfowl Populations Breeding in the Northern Great Plains. Climatic Change 40:343–369.

Soykan, C. U., J. Sauer, J. G. Schuetz, G. S. LeBaron, K. Dale, and G. M. Langham (2016). Population trends for North American winter birds based on hierarchical models. Ecosphere 7:e01351.

Stanton, R. L., C. A. Morrissey, and R. G. Clark (2018). Analysis of trends and agricultural drivers of farmland bird declines in North America: A review. Agriculture, Ecosystems & Environment 254:244–254.

Steen, V. A., S. K. Skagen, and C. P. Melcher (2016). Implications of Climate Change for Wetland-Dependent Birds in the Prairie Pothole Region. Wetlands 36:445–459.

Sullivan, B. L., J. L. Aycrigg, J. H. Barry, R. E. Bonney, N. Bruns, C. B. Cooper, T. Damoulas, A. A. Dhondt, T. Dietterich, A. Farnsworth, D. Fink, et al. (2014). The eBird enterprise: An integrated approach to development and application of citizen science. Elsevier 169:31–40.

Thogmartin, W. E., J. R. Sauer, and M. G. Knutson (2004). A Hierarchical Spatial Model of Avian Abundance with Application to Cerulean Warblers. Ecological Applications 14:1766–1779.

Thorson, J. T., C. L. Barnes, S. T. Friedman, J. L. Morano, and M. C. Siple (2023). Spatially varying coefficients can improve parsimony and descriptive power for species distribution models. Ecography 2023:e06510.

Ver Hoef, J. M., E. E. Peterson, M. B. Hooten, E. M. Hanks, and M.-J. Fortin (2018). Spatial autoregressive models for statistical inference from ecological data. Ecological Monographs 88:36–59.

Wilson, S., S. L. LaDeau, A. P. Tøttrup, and P. P. Marra (2011). Range-wide effects of breeding- and nonbreeding-season climate on the abundance of a Neotropical migrant songbird. Ecology 92:1789–1798.

Wilson, S., A. C. Smith, and I. Naujokaitis-Lewis (2018). Opposing responses to drought shape spatial population dynamics of declining grassland birds. Diversity and Distributions 24:1687–1698.

Wright, W. J., K. M. Irvine, T. J. Rodhouse, and A. R. Litt (2021). Spatial Gaussian processes improve multi-species occupancy models when range boundaries are uncertain and nonoverlapping. Ecology and Evolution 11:8516–8527.

Figures and captions

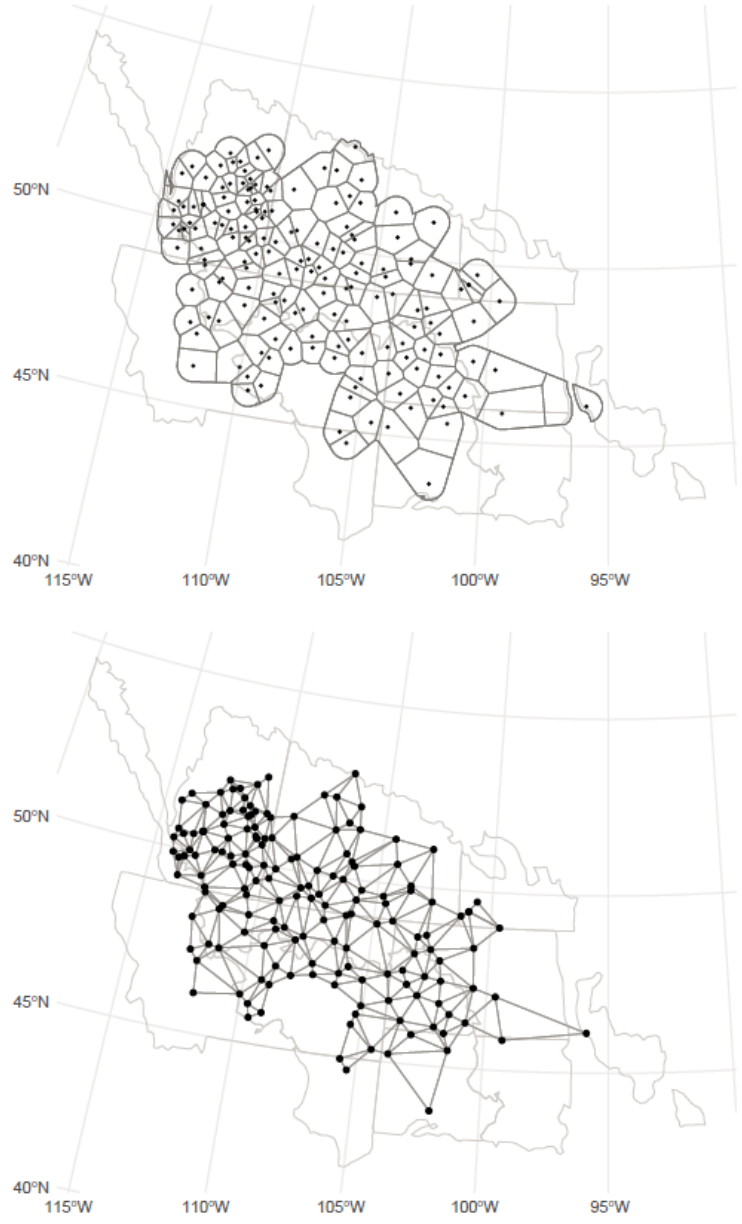

Figure 1. BBS route start locations (points) for routes on which Baird's Sparrow was observed (2006-2021), demonstrating the process used to identify the discrete neighbor relationships for the iCAR and BYM spatial models. The top panel shows the Voronoi tessellated surface used to assign the intervening space to the nearest BBS route start location, which is intersected with a concave polygon and the standard BBS strata (State/Provinces/Territories by Bird Conservation Regions). The lower panel shows routes considered neighbors using lines linking points that share an edge separating their associated Voronoi polygons.

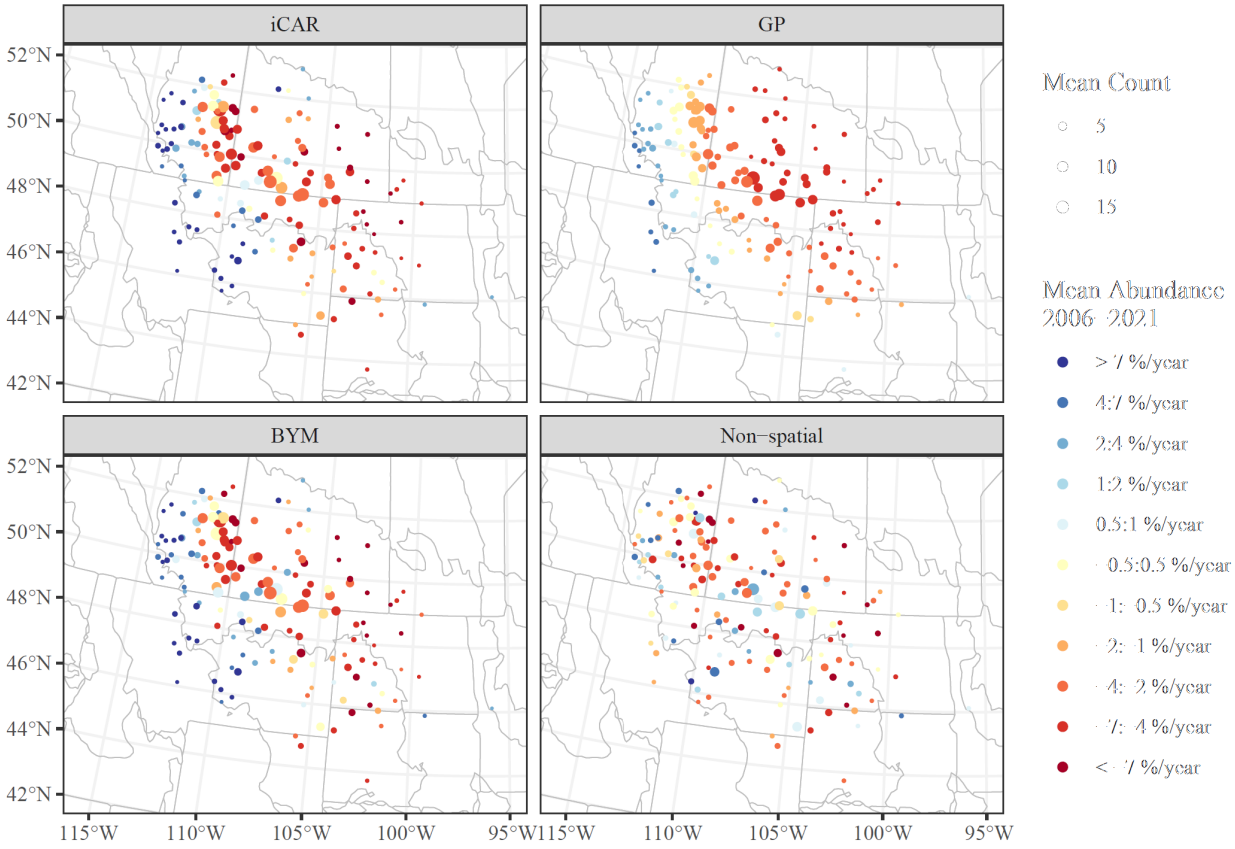

Figure 2. Estimates of trend (colours) and mean relative abundance (size of the points) for Baird's Sparrow populations on BBS routes from 2006-2021, from three spatially explicit models (iCAR, GP, and BYM) and one non-spatial model. Points with warm colours (reds) represent routes with decreasing counts through time, points with cool colours (blues) represent routes with increasing counts through time. The three spatially explicit models suggest very similar spatial patterns in trends, although the GP model suggests smoother spatial variation in trend than either the iCAR or BYM models. Grey lines within the maps represent boundaries of provinces/states and Bird Conservation Regions.

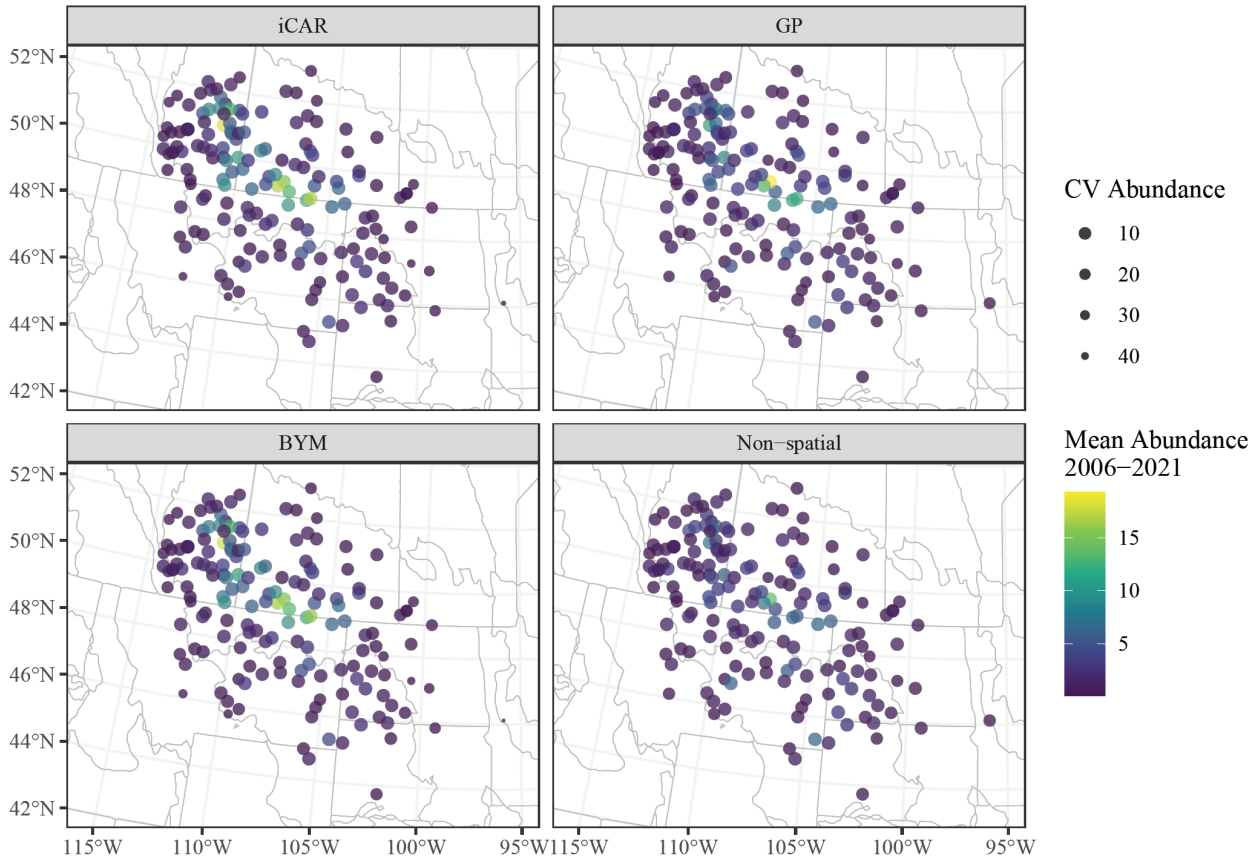

799

800 Figure 3. Estimates of mean relative abundance (colours) and the Coefficient of Variation for the
801 estimates (CV = size) for Baird's Sparrow populations on BBS routes from 2006-2021, from three
802 spatially explicit models and one non-spatial model. Points with brighter colours (greens and yellows)
803 represent routes with higher estimated mean counts, points with more precise estimates of abundance
804 (smaller CV) are larger. The iCAR and BYM models estimate almost identical spatial patterns in
805 abundance with a relatively clear peak in the center of the species' range, and relatively smoother spatial
806 variation than either the GP or the non-spatial model.

807

808

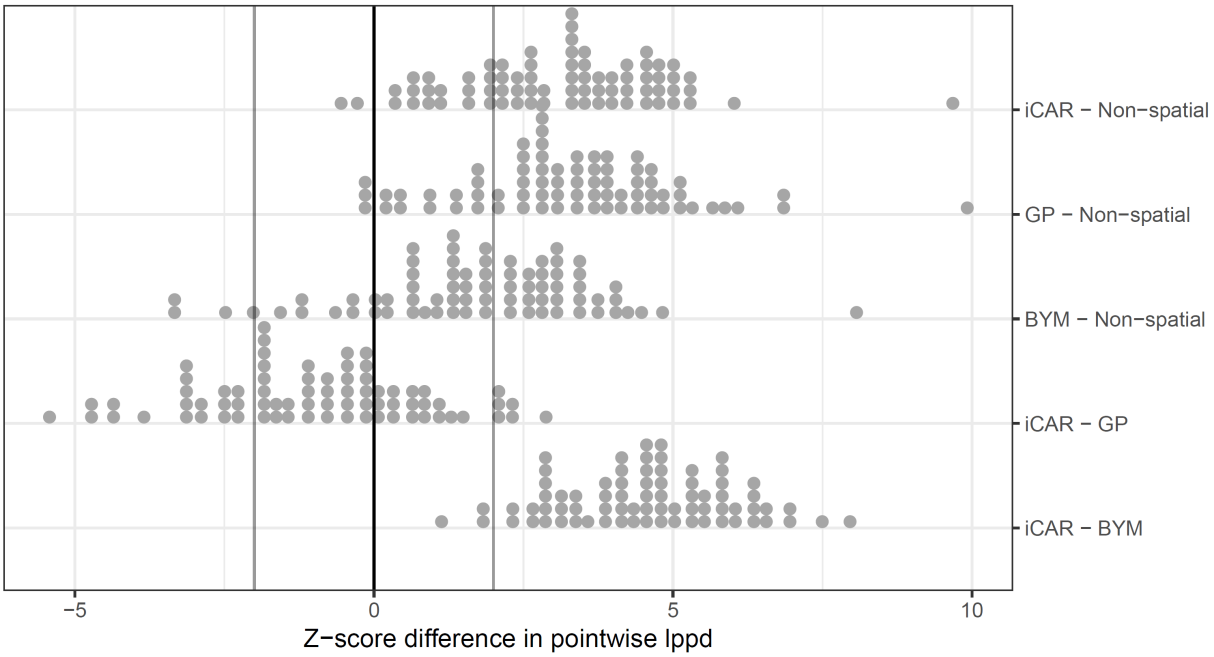

Figure 4. Leave Future Out (LFO) cross-validation results for 71 small-range species from the BBS database, comparing among the four different models. The stacked dot-plots represent species-level summaries of the differences in lppd between pairs of models. Each point represents one species for a given model comparison. Z-score values on the x-axis represent the difference between the lppd for the two models indicated on the y-axis. Z-scores > 0 (points that fall to the right of the black vertical line) represent species for which the predictive accuracy of the first model is higher than that of the second model (e.g., all but two species in the iCAR vs Non-spatial comparison), and vice versa. Z-scores > 2 or < -2 (points that fall to the right or left of the vertical dark gray lines, respectively) represent species for which the mean of the differences between the two models are clear and could be considered "significant" in some statistical frameworks. The top three dot-plots show the comparisons between each of the three spatial models and the non-spatial model. The lower two plots compare the predictive accuracy among the three spatial models and show that the iCAR model out-performs the BYM model for all species, and that the GP model out-performs the iCAR model for some species but not for others .

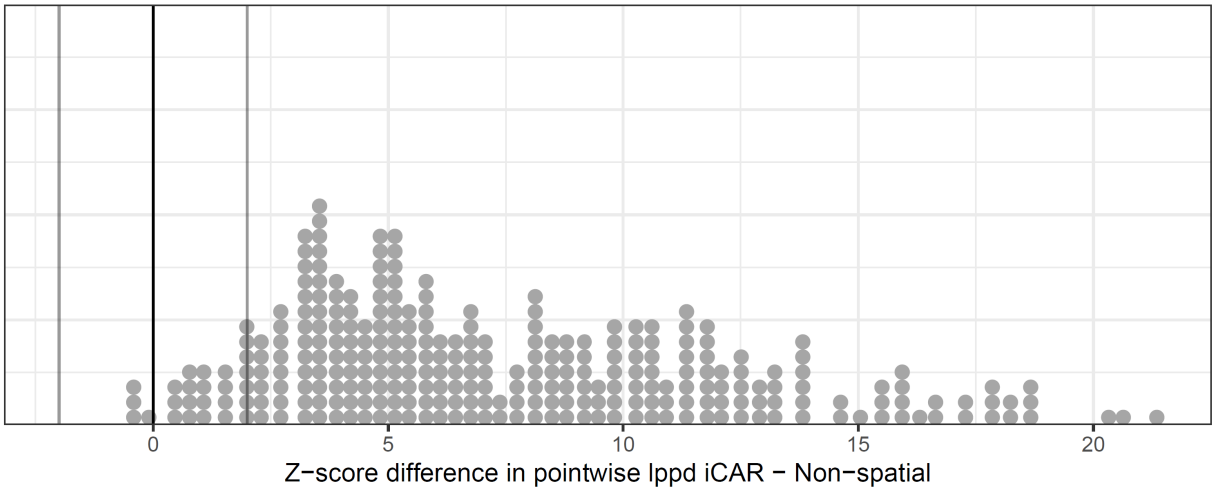

Figure 5. Leave Future Out (LFO) cross-validation results for all 287 species (including the 71 species results in Figure 4), comparing the iCAR spatial model and the non-spatial model. The stacked dot-plots represent species-level summaries of the differences in lppd between the two models. Each point represents one species. Z-score values represent the difference between the lppd for the two models accounting for the variation across all counts, and the stacked dots form a histogram. Points that fall to the right of the black vertical line represent species for which the predictive accuracy of the spatial model is higher than that of the non-spatial model. The iCAR spatial model outperforms the non-spatial model for all but four species. For those four species, the predictive accuracy of the two models is very similar and does not approach -2, which would support a clear difference between the two models in favour of the non-spatial model.

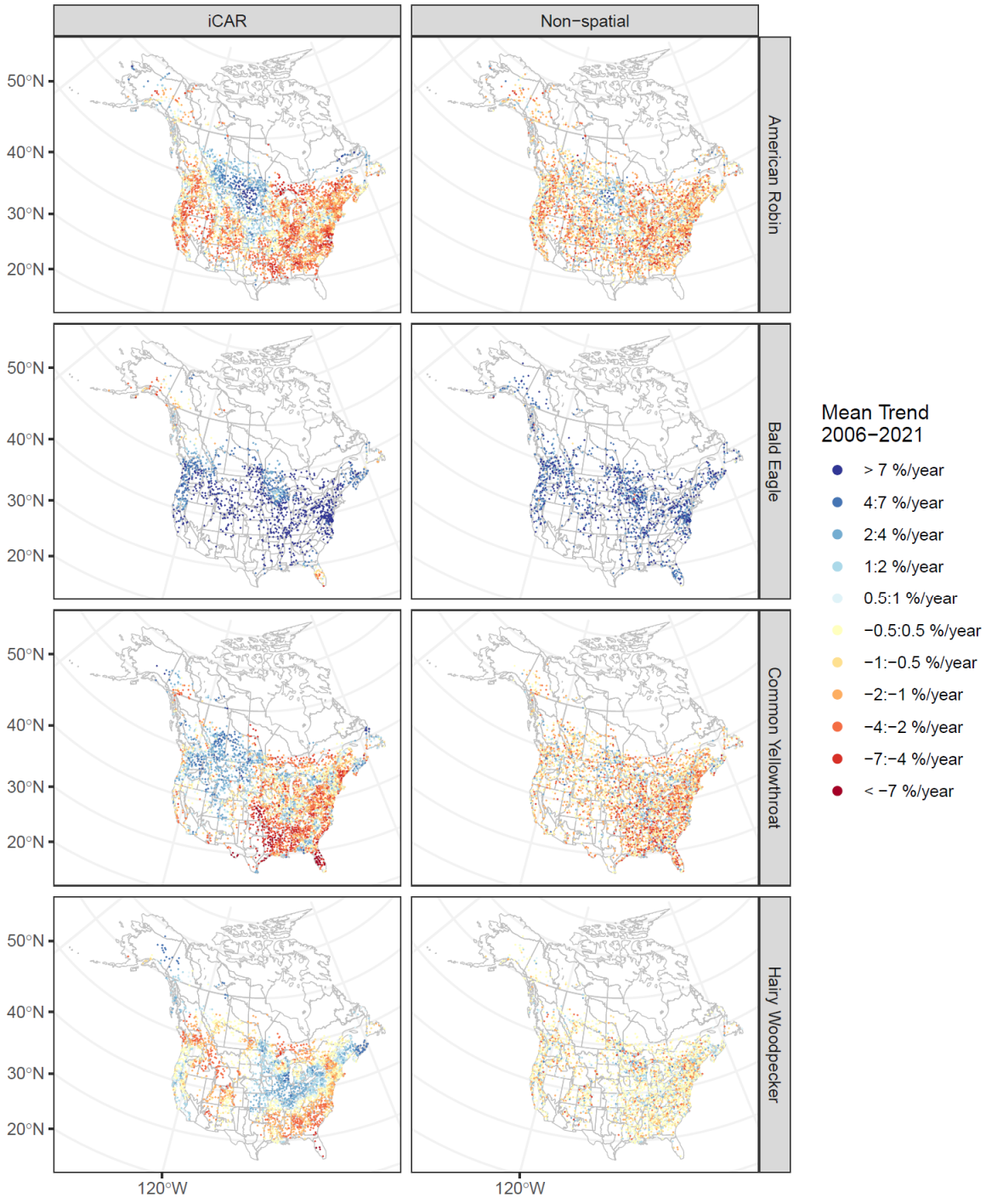

Figure 6. Examples of the spatial patterns in estimated route-level trends for four broad-range species from an iCAR spatial model (left column) compared to trends estimated from an otherwise identical, non-spatial version of the model (right column). All points are the same size in this plot because the mean abundances vary too much among species to display meaningful variation in this plot.

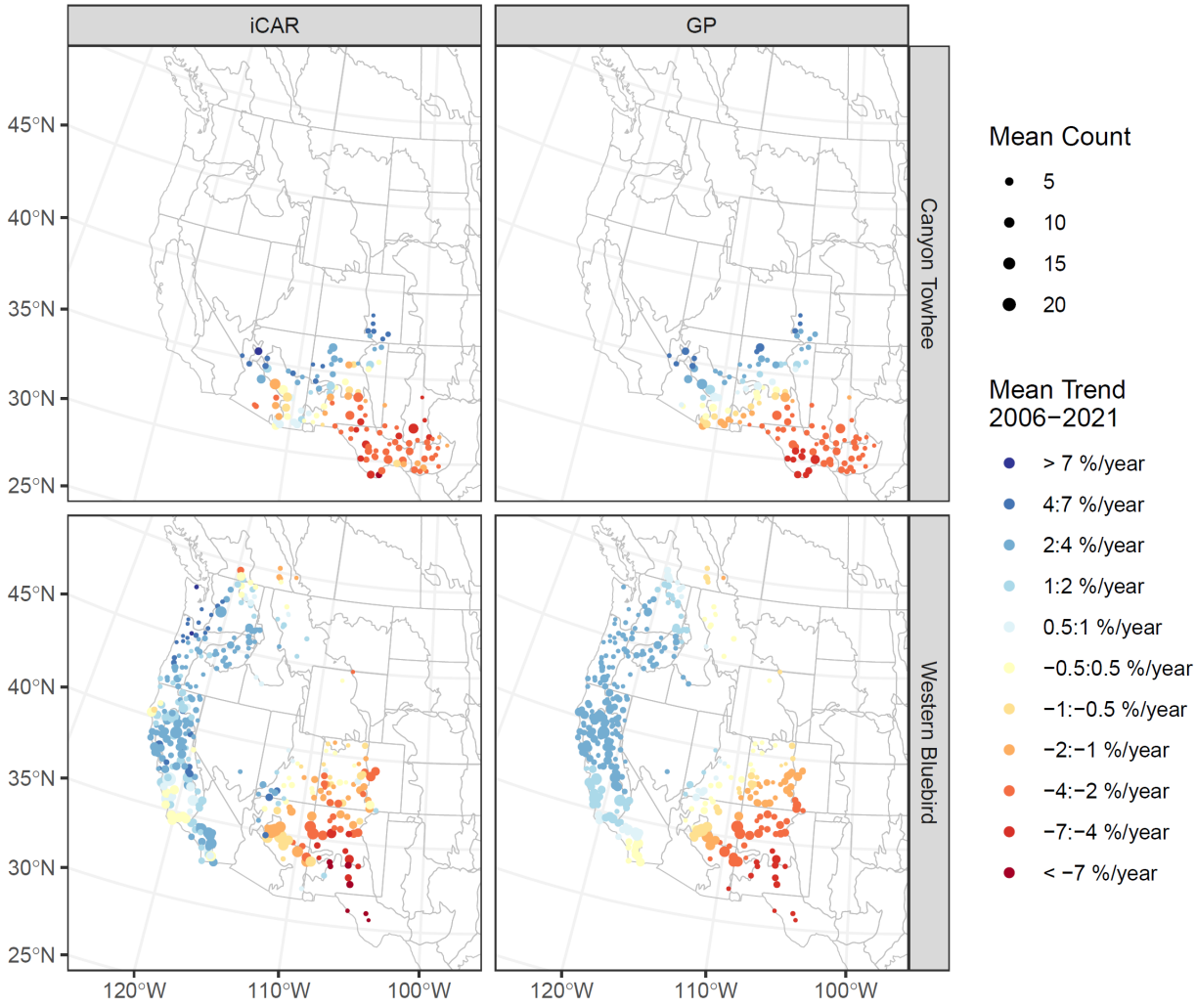

Figure 7. An example illustrates that the spatial patterns in estimated trends for iCAR and GP models are quite similar, even when one of the models strongly out-performs the other in a cross-validation analysis. For the Canyon Towhee (*Melozone fusca*), the GP model clearly out-performs the iCAR model in predictive accuracy (z-score comparison iCAR – GP = -4.3, Figure 4). For the Western Bluebird (*Sialia mexicana*), the iCAR model out-performs the GP model in predictive accuracy (z-score comparison iCAR – GP = 2.9, Figure 4). Despite the relatively strong difference in predictive accuracy, the spatial patterns are quite similar for both models.

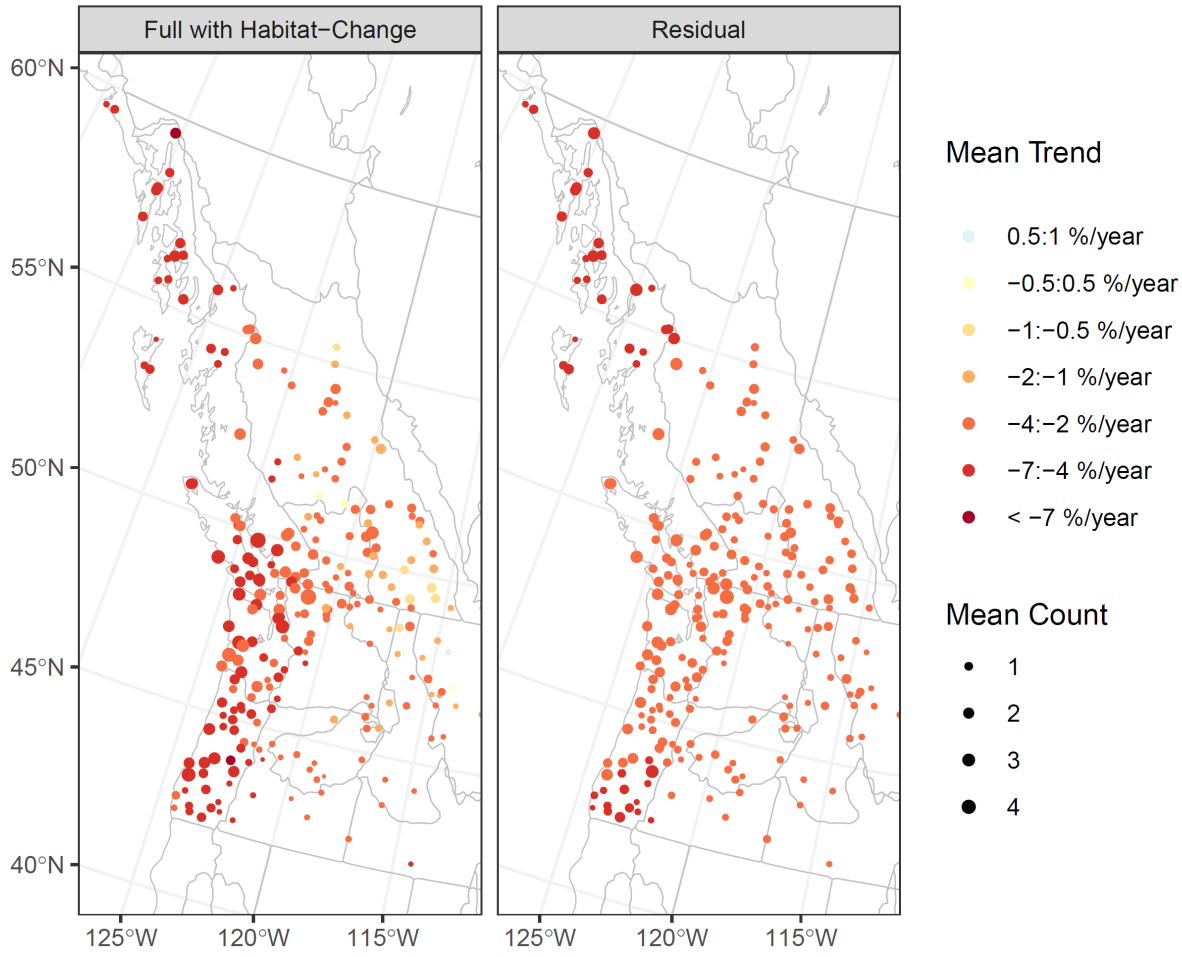

Figure 8. Map of route-level trend estimates for Rufous Hummingbird (*Selasphorus rufus*) from 2006-2021. The colours represent trends estimated from the model including effects of habitat change (left panel) and the residual spatially explicit estimate of trend, after removing the effects of habitat change (right panel). Habitat change appears to be driving most of the variation in trends within the core latitudes of the species range (45°-55° N). The faster rates of decline (darker red) in the western regions and the slower rates of decline (lighter yellow) in the east are evident in the left panel that includes the effects of habitat and missing from the panel on the right.

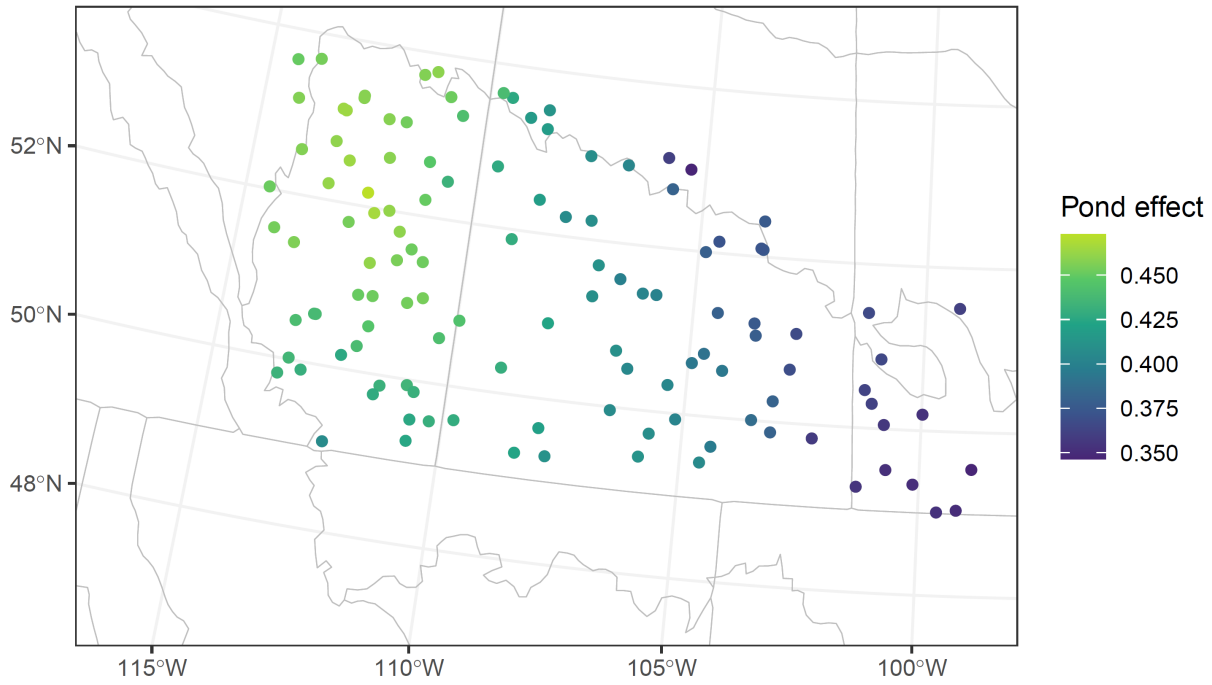

Figure 9. A map of the spatial variation in the effects of annual fluctuations in available habitat (ponds) on the expected counts of Horned Grebe during BBS routes (1975-2017). The pond effect was estimated as a spatially varying coefficient using the iCAR structure among routes and was strongest in the western prairies. Pond effect represents the log-scale effect of annual variation in the number of ponds surrounding a BBS route in a given year on the annual expected count after adjusting for long-term trends, observer-effects, and the other parameters included in all of the models we used.